

Multiplexed Fluorescence Imaging of ERK and Akt Activities and Cell-cycle Progression

Gembu Maryu¹, Michiyuki Matsuda^{1,2}, and Kazuhiro Aoki^{3,4,5*}

¹Laboratory of Bioimaging and Cell Signaling, Graduate School of Biostudies, Kyoto University, Sakyo-ku, Kyoto 606-8501, Japan, ²Department of Pathology and Biology of Diseases, Graduate School of Medicine, Kyoto University, Sakyo-ku, Kyoto 606-8501, Japan, ³Imaging Platform for Spatio-Temporal Information, Graduate School of Medicine, Kyoto University, Sakyo-ku, Kyoto 606-8501, Japan, ⁴Division of Quantitative Biology, Okazaki Institute for Integrative Bioscience, National Institute for Basic Biology, National Institutes of Natural Sciences, Okazaki, Aichi 444-8787, Japan, ⁵Department of Basic Biology, Faculty of Life Science, SOKENDAI (Graduate University for Advanced Studies), Myodaiji, Okazaki, Aichi 444-8787, Japan

ABSTRACT. The Ras-ERK pathway controls cell proliferation and differentiation, whereas the PI3K-Akt pathway plays a role in the process of cell-cycle progression and cell survival. Both pathways are activated by many stimuli such as epidermal growth factor (EGF), and coordinately regulate each other through cross-talk. However, it remains unclear how cells accommodate the dynamics and interplay between the Ras-ERK and PI3K-Akt pathways to regulate cell-fate decisions, mainly because of the lack of good tools to visualize ERK and Akt activities simultaneously in live cells. Here, we developed a multiplexed fluorescence system for imaging ERK and Akt signaling and the cell-cycle status at the single cell level. Based on the principle of the kinase translocation reporter (KTR), we created Akt-FoxO3a-KTR, which shuttled between nucleus and cytoplasm in a manner regulated by Akt phosphorylation. To simultaneously measure ERK, Akt and the cell-cycle status, we generated a polycistronic vector expressing ERK-KTR, Akt-FoxO3a-KTR, a cell-cycle reporter and a nuclear reporter, and applied linear unmixing to these four images to remove spectral overlap among fluorescent proteins. The specificity and sensitivity of ERK-KTR and Akt-FoxO3a-KTR were characterized quantitatively. We examined the cellular heterogeneity of relationship between ERK and Akt activities under a basal or EGF-stimulated condition, and found that ERK and Akt were regulated in a highly cooperative and cell-cycle-dependent manner. Our study provides a useful tool for quantifying the dynamics among ERK and Akt activities and the cell cycle in a live cell, and for addressing the mechanisms underlying intrinsic resistance to molecularly targeted drugs.

Key words: ERK, Akt, Fluorescence imaging

Introduction

The Ras-Raf-mitogen-activated protein/extracellular-signal-regulated kinase kinase (MEK)-extracellular signal-regulated kinases (ERK) signaling pathway (hereafter the Ras-ERK pathway) plays an essential role in cell proliferation and differentiation (Qi and Elion, 2005). The phosphatidylinositol 3 kinase (PI3K)-Akt-mammalian target of rapamycin (mTOR) signaling pathway (referred to as the PI3K-Akt

pathway) has a main role in cell motility, survival, and metabolism (Brunet *et al.*, 1999). Constitutive activation of the Ras-ERK and PI3K-Akt pathways leads to the development of tumors, and indeed, gain-of-function mutations in these pathways are frequently found in various types of human malignant tumors (Pylayeva-Gupta *et al.*, 2011; She *et al.*, 2008). Thus, these pathways have been targeted in anti-cancer therapy (Polivka Jr. and Janku, 2014; Roberts and Der, 2007).

The Ras-ERK and PI3K-Akt pathways were originally modeled as linear signaling cascades, yet accumulating evidence indicates that they intersect to regulate each other and co-regulate downstream functions (Mendoza *et al.*, 2011). For instance, Akt phosphorylates CRaf at Ser259,

*To whom correspondence should be addressed: Kazuhiro Aoki, Okazaki Institute for Integrative Bioscience, National Institute for Basic Biology, National Institutes of Natural Sciences, Okazaki, Aichi 444-8787, Japan.
Tel: +81-564-59-5235
E-mail: k-aoki@nibb.ac.jp

maintaining CRaf in a closed inactive conformation (Zimmermann and Moelling, 1999), while ERK phosphorylates Grb2-associated binder 1 (GAB1), an adapter protein, and inhibits GAB1-mediated recruitment of PI3K to the epidermal growth factor (EGF) receptor (Lehr *et al.*, 2004). More strikingly, several studies have implied that feedback regulations and cross-talk regulations of the Ras-ERK pathway and the PI3K-Akt pathway neutralize molecularly targeted drug efficiency in tumor cells, a phenomenon known as intrinsic resistance (Friday *et al.*, 2008; Prahallad *et al.*, 2012; Won *et al.*, 2012). In line with these evidences, we have recently reported that a quantitative kinetic simulation model including feedback and cross-talk regulations in these pathways enabled us to predict the difference of MEK inhibitor sensitivity to KRas-mutant or BRAf-mutant cancer cells (Fujita *et al.*, 2014). Therefore, understanding the feedback and cross-talk regulations of these pathways is of critical importance for optimizing therapeutic outcomes using molecularly targeted drugs.

To dissect feedback and cross-talk regulations between signaling pathways, live cell imaging is the most straightforward approach; to analyze the feedback and cross-talk regulations, fast sampling with acute perturbations is inherently required (Inoue and Meyer, 2008). To meet these requirements, we have developed and employed biosensors based on the principle of Förster resonance energy transfer (FRET) (Fujita *et al.*, 2014; Miura *et al.*, 2014). To date, most FRET applications have been limited to monitoring only a single target, or at most two targets, and have been limited by technical difficulties (Ai *et al.*, 2008; Niino *et al.*, 2009). More recently, Covert and colleagues developed single fluorophore biosensors for kinase activity named kinase translocation reporters (KTRs), and visualized multiple kinase activities, i.e., ERK, JNK and p38, in live cells (Regot *et al.*, 2014). The KTRs make it possible to monitor kinase activity from their nucleocytoplasmic shuttling. This prompted us to investigate ERK and Akt activities simultaneously at the single cell level.

In this study, we developed Akt-FoxO3a-KTR to visualize Akt activity, and established a multiplexed imaging system for monitoring ERK and Akt activities and cell-cycle progression with a fluorescent ubiquitination-based cell-cycle indicator (Fucci) system (Sakaue-Sawano *et al.*, 2008a). The specificity and sensitivity of Akt-FoxO3a-KTR and ERK-KTR were confirmed with the use of inhibitors and biochemical assays. By simultaneous visualization of ERK and Akt activities and the cell-cycle status, we found a strong correlation of basal level, EGF responsiveness, and cross-talk regulations between ERK and Akt at the single cell level. Further, basal ERK and Akt activities were regulated in a cell-cycle-dependent manner, providing a new insight into the cell-cycle-dependent regulation of ERK and Akt.

Material and Methods

Plasmids

The plasmids encoding nuclear marker, Histone-H2B (H2B)-iRFP, and the S/G₂/M cell-cycle marker, mCherry-hGem, were kind gifts from Dr. Miyanari (National Institute for Basic Biology, Aichi, Japan) and Dr. Miyawaki (RIKEN, Saitama, Japan) (Sakaue-Sawano *et al.*, 2008b), respectively. The cDNA of the ERK activity reporter, ERK-KTR (Regot *et al.*, 2014), was synthesized by annealing sense- and antisense-oligo DNA nucleotides, and subcloned into a pCSIIneo-mKO vector, generating pCSIIneo-ERK-KTR-mKO. For the Akt activity reporter, the cDNA of human *FoxO3a* genes was amplified from a cDNA pool obtained from mRNA of HeLa cells, and the His-to-Arg mutation at the 212 position was introduced with a two-step overlap PCR. The cDNAs of truncated FoxO3a were generated by PCR and subcloned into pCAGGS-EGFP vector to generate pCAGGS-FoxO3a-EGFP, pCAGGS-Akt-FoxO3a-KTR-EGFP (1–401 a.a.), and pCAGGS-FoxO3a (241–401 a.a.)-EGFP. pCX4puro-LDR, pCAGGS-Flag-CRaf-FKBP, and pCAGGS-GST-FKBP-iSH2 have been described previously (Aoki *et al.*, 2011; Miura *et al.*, 2014).

To construct a polycistronic vector expressing H2B-iRFP, mCherry-hGem, ERK-KTR-mKO, and Akt-FoxO3a-KTR-EGFP simultaneously, these cDNAs were connected with cDNAs of a self-cleaving P2A peptide (GSGATNFSLLKQAGDDVEENPGP) by PCR. cDNAs of three P2A peptides in between reporters contained nonsense mutations to prevent unexpected annealing of PCR primers. The cDNA of tandemly connected reporter genes was inserted into the *piggyBac* donor vector pPBbsr to generate pHGEA (Fig. 2B).

Cells, reagents, and antibodies

HeLa cells were purchased from the Human Science Research Resources Bank (Osaka, Japan), and maintained in DMEM (Sigma-Aldrich, St. Louis, MO) supplemented with 10% fetal bovine serum at 37°C under 5% CO₂. To establish a stable cell line, HeLa cells were co-transfected with pHGEA and pCMV-mPBbase (neo-) encoding the *piggyBac* transposase provided by Dr. Bradley (Wellcome Trust Sanger Institute, Cambridge, UK) (Yusa *et al.*, 2009) at a ratio of 3:1 by using Polyethylenimine Max (Polyscience Inc., Warrington, PA). Expressing cells were selected with 20 µg/mL blasticidin (InvivoGen, San Diego, CA) for at least 7 days. Bulk populations of selected cells were used in this study.

Epidermal growth factor (EGF) was purchased from Sigma-Aldrich (St. Louis, MO). PD184352 and AZD5363 were from Toronto Research Chemicals (Ontario, Canada) and Cayman Chemical (Ann Arbor, MI), respectively. Anisomycin, JNK inhibitor VIII and PI-103 were purchased from Calbiochem (La Jolla, CA). SB203580 was from Selleckchem (Boston, MA).

Anti-mCherry rabbit polyclonal antibody, anti-mKO2 rabbit polyclonal antibody, and anti-GFP mouse monoclonal antibody were obtained from Abcam (Cambridge, UK), MBL (Aichi,

Japan), and Clontech Laboratories Inc. (Mountain View, CA), respectively. Anti-Akt (pan) rabbit monoclonal antibody (C67E7), anti-phospho-Akt (Ser473) mouse monoclonal antibody (587F11), anti-ERK rabbit monoclonal antibody (137F5), and anti-pERK (Thr202/Tyr204) mouse monoclonal antibody (E10) were purchased from Cell Signaling Technology (Danvers, MA). The IRDye680LT- and IRDye800CW-conjugated anti-rabbit and anti-mouse immunoglobulin G secondary antibodies were obtained from LI-COR (Lincoln, NE).

Time-lapse imaging

HeLa cells expressing reporters stably or transiently were plated on 35 mm glass-base dishes (Asahi Techno Glass, Tokyo, Japan) or 35 mm 4 section glass-base dishes (Greiner, Frickenhausen, Germany), and starved for 3 hours with FluoroBrite D-MEM (LifeTechnologies, Carlsbad, CA) supplemented with 1% GlutaMAX (LifeTechnologies) and 0.1% bovine serum albumin (BSA). Imaging was performed with an inverted microscope IX81 (Olympus, Tokyo, Japan) equipped with a UPlanSApo 60x/1.35 objective lens (Olympus), a Retiga 4000R cooled CCD camera (Photometrics, Tucson, AZ), a Spectra-X light engine (Lumencor Inc., Beaverton, OR), an IX2-ZDC laser-based autofocusing system (Olympus), a MAC5000 controller for filter wheels and XY stage (Ludl Electronic Products, Hawthorne, NY), and an incubation chamber (Tokai Hit, Shizuoka, Japan). The filters and dichroic mirrors used for time-lapse imaging were as follows: for iRFP, 632/22 excitation filters (Semrock, Rochester, NY), a FF408/504/581/667/762 dichroic mirror (Semrock) and 700/LP-25 emission filters (Semrock); for mCherry, a 580/20 excitation filter (Semrock), 20/80 beamsplitter dichroic mirror (Chroma), and 641/75 emission filter (Semrock); for mKO, a 543/3 excitation filter (Semrock), 20/80 beamsplitter dichroic mirror (Chroma), and 563/9 emission filter (Semrock); for EGFP imaging, a 475/28 excitation filter, 20/80 beamsplitter dichroic mirror (Chroma), and 542/27 emission filter (Semrock). The microscope was controlled by MetaMorph software (Molecular Devices, Sunnyvale, CA).

Immunoblotting

HeLa cells were lysed in 1x SDS sample buffer (1 M Tris-HCl pH 6.8, 50% glycerol, 10% SDS, 0.2% Bromo Phenol Blue, and 10% 2-mercaptoethanol). After sonication, the samples were separated by SDS-polyacrylamide gel electrophoresis (PAGE) and transferred to polyvinylidene difluoride membranes (Millipore, Billerica, MA). After blocking with skim milk (Morinaga, Tokyo, Japan) for 1 hour, the membranes were incubated with primary antibodies diluted in Odyssey blocking buffer (LI-COR), followed by secondary antibodies diluted in Odyssey blocking buffer. Proteins were detected by an Odyssey Infrared scanner (LI-COR) and analyzed by using the Odyssey software.

Image analysis and linear unmixing

After background pixel intensities were subtracted for each time point, linear unmixing was performed as follows (Niino *et al.*, 2009; Zimmermann *et al.*, 2003). In brief, HeLa cells expressing each fluorescent protein ($i=1$ (EGFP), $i=2$ (mKO), $i=3$ (mCherry), and $i=4$ (iRFP)) were imaged with each channel for fluorescent protein ($j=1$ (EGFP Ch.), $j=2$ (mKO Ch.), $j=3$ (mCherry Ch.), and $j=4$ (iRFP Ch.)). The raw fluorescence intensity of fluorescent protein i with fluorescence channel j is represented as F_{ij} . The ij component of normalized spectral matrix \mathbf{A} is defined as follows:

$$A_{ij} = \frac{F_{ij}}{F_{i,j=i}}. \quad (\text{eq. 1})$$

Thus, A_{ij} indicates to what extent the fluorescence intensity of protein i leaks into fluorescence channel j . \mathbf{A} was obtained experimentally. By using the normalized spectral matrix \mathbf{A} , the raw image vector \mathbf{R} , which is obtained with fluorescence channel i ($i=1\sim 4$), can be described as follows:

$$\mathbf{A} \cdot \vec{\mathbf{T}} = \vec{\mathbf{R}}, \quad (\text{eq. 2})$$

where \mathbf{T} is a vector of true images of each fluorescent protein j ($j=1\sim 4$). Finally, the true fluorescence images \mathbf{T} are obtained by multiplying the inverse matrix of \mathbf{A} on the left of the equation 2 as follows:

$$\mathbf{T} = \mathbf{A}^{-1} \cdot \vec{\mathbf{R}}. \quad (\text{eq. 3})$$

The inverse matrix of \mathbf{A} was calculated from experimentally-determined \mathbf{A} with MATLAB software (MathWorks, Natwick, MA), and true images \mathbf{T} were obtained by multiplying values of the inverse matrix of \mathbf{A} in MetaMorph.

Unmixed images were used for further image analysis. For each cell, two regions of interest (ROIs) were set at the nucleus and cytoplasm, and their positions were manually registered so that these ROIs remained in the nucleus and cytoplasm. Average fluorescence intensities in ROIs were exported, and the cytoplasm/nucleus (C/N) ratio values of Akt-FoxO3a-KTR and ERK-KTR were calculated by dividing the average intensity at the cytoplasm by that at the nucleus in Excel software (Microsoft Corporation, Redmond, WA).

Results

Development of a kinase translocation reporter for Akt, Akt-FoxO3a-KTR

To visualize ERK and Akt activities and the cell-cycle progression simultaneously at the single cell level, we first developed a genetically-encoded single-fluorophore Akt activity reporter. For this purpose, we focused on the kinase translocation reporter (KTR) system, in which kinase activity is converted into a nucleocytoplasmic shuttling event,

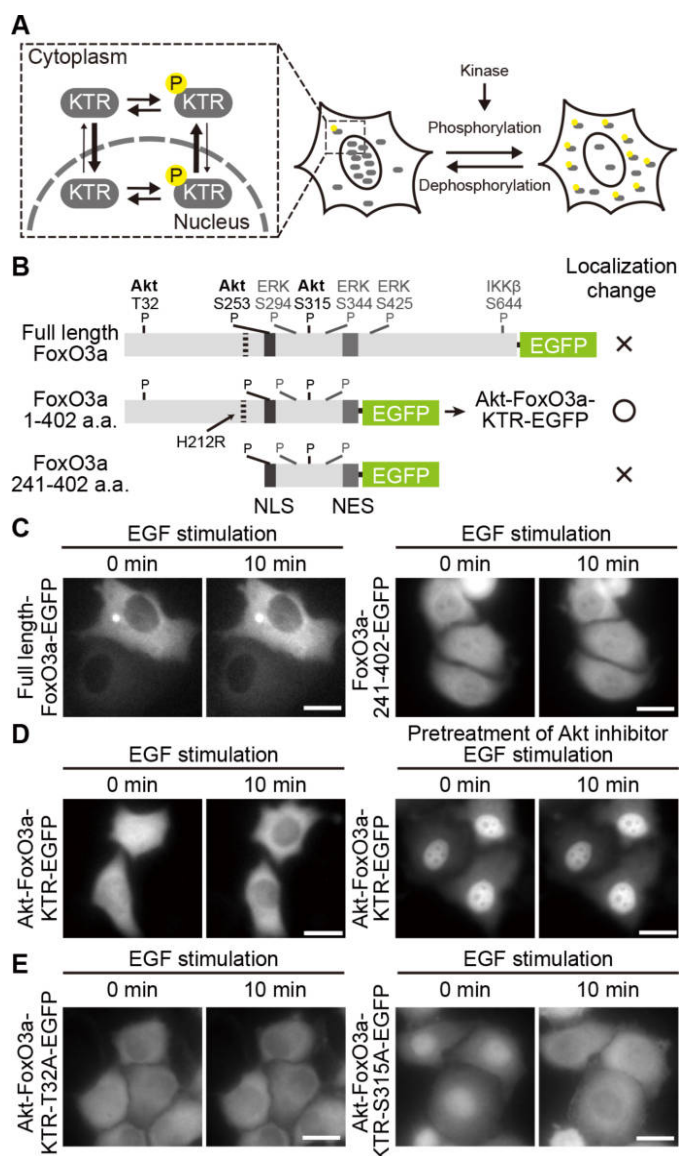


Fig. 1. Development of an Akt activity reporter, Akt-FoxO3a-KTR. (A) Schematic representation of the phosphorylation-dependent subcellular distribution of the kinase translocation reporter (KTR). Under low kinase activity, the non-phosphorylated biosensors are predominantly localized at the nucleus, whereas upon kinase activation, the biosensors are phosphorylated and exported to the cytoplasm. (B) Structure of various versions of Akt-FoxO3a-KTR-EGFP. All are composed of human FoxO3a mutants (upper, full length; middle, 1–402 a.a.; lower, 241–402 a.a.) followed by EGFP. Phosphorylation sites and corresponding kinases are represented with H212R mutation, which leads to the loss of DNA binding activity of FoxO3a. The reporter including the 1–402 a.a. region of FoxO3a showed the highest dynamic range, and was designated Akt-FoxO3a-KTR-EGFP. (C) Representative images of full length FoxO3a-EGFP (left) and FoxO3a (241–402 a.a.)-EGFP (right) before and after EGF stimulation. (D) Representative images of Akt-FoxO3a-KTR-EGFP before and after EGF treatment with or without 20 μ M AZD5363, an Akt inhibitor. (E) Representative images of Akt-FoxO3a-KTR-T32A-EGFP (left) and Akt-FoxO3a-KTR-S315A-EGFP (right) before and after EGF stimulation. Scale bar, 20 μ m.

enabling the measurement of multiple kinase activities in a single cell (Regot *et al.*, 2014). KTR technology consists of a nuclear localization signal (NLS) and nuclear export signal (NES) that are negatively and positively regulated by phosphorylation, respectively; unphosphorylated KTR proteins are localized at the nucleus, whereas phosphorylated KTR proteins are exported to the cytoplasm (Fig. 1A). A transcription factor, FoxO3a, has the same naturally occurring arrangement of NLS, NES and phosphorylation sites of Akt within the central region of FoxO3a (Fig. 1B), and shows nucleocytoplasmic shuttling in a manner dependent on phosphorylation by Akt (Obsil and Obsilova, 2008). Therefore, we exploited human FoxO3a for the development of Akt-FoxO3a-KTR. First, a His residue in the 212 position was substituted to Arg to eliminate the transcrip-

tional activity of FoxO3a (Tran *et al.*, 2002). Next, we investigated and observed nucleocytoplasmic shuttling of full length FoxO3a fused with EGFP upon EGF stimulation (Fig. 1B). Since FoxO3a has an IKK β phosphorylation site that induces protein localization change regardless of the state of Akt phosphorylation (Hu *et al.*, 2004), we developed deletion mutants of FoxO3a. The full length of FoxO3a fused with EGFP was localized at the cytoplasm in HeLa cells regardless of EGF stimulation, and FoxO3a (241–402 a.a.)-EGFP did not show any nucleocytoplasmic shuttling upon EGF stimulation, even for the typical KTR motif located in the central region (Fig. 1C). The deletion of only the C-terminal region (from 402 a.a. to the end) resulted in more clear nucleocytoplasmic shuttling (Fig. 1D, left). We selected the region from 1–402 a.a. of

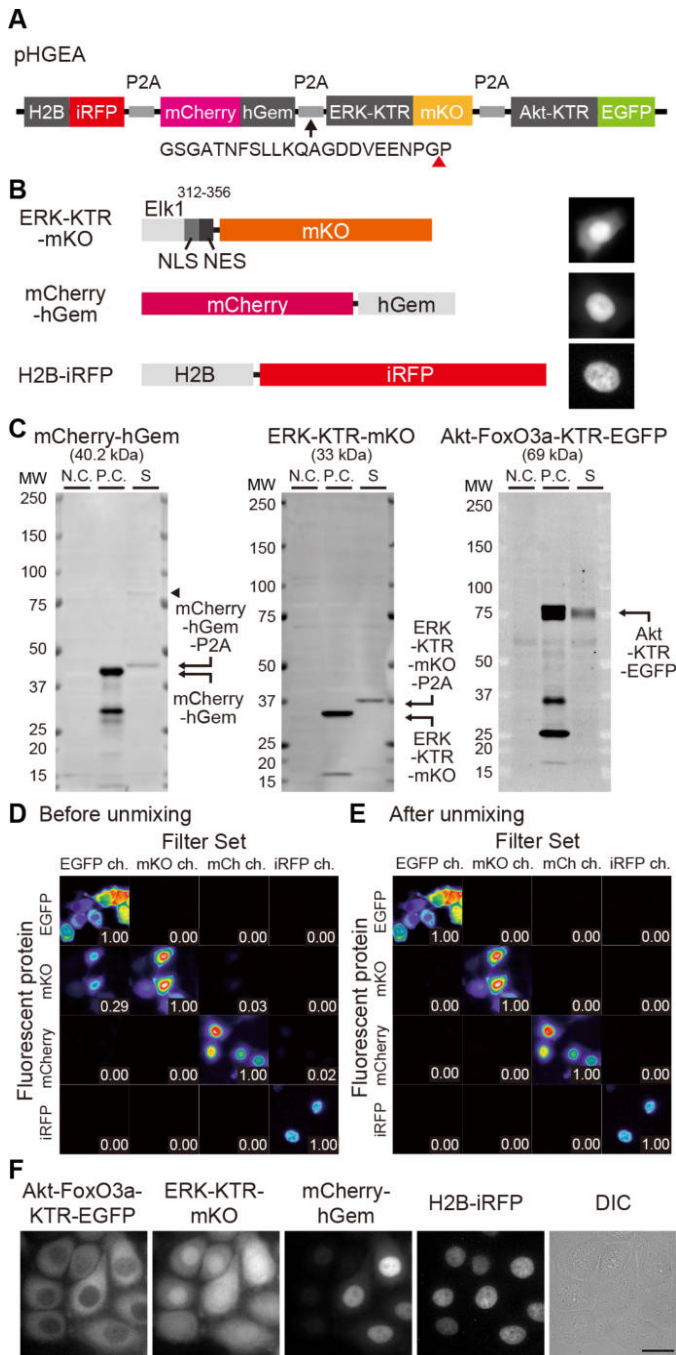


Fig. 2. Establishment of the multicolor imaging system. (A) Schematic representation of the HGEA reporter, consisting of H2B-iRFP, mCherry-hGem, ERK-KTR-mKO, and Akt-FoxO3a-KTR-EGFP. They are connected with self-cleaving P2A peptides, so that these reporters are expressed separately. A red arrowhead indicates the cleaving site of P2A peptide. (B) Structure (left) and representative localization of ERK-KTR-mKO, mCherry-hGem, and H2B-iRFP. HeLa cells expressing each reporter were imaged with an epifluorescence microscope. (C) HeLa cells stably expressing mCherry-hGem, ERK-KTR-mKO, and Akt-FoxO3a-KTR-EGFP were lysed and analyzed by immunoblotting with anti-mCherry (left), anti-mKO (middle), and anti-EGFP antibodies (right), respectively. N.C. indicates the negative control, which was the cell lysate from parental HeLa cells. P.C. indicates the positive control, which was the cell lysate from HeLa cells transiently expressing each reporter. S indicates a sample prepared from HeLa cells stably expressing four reporters by the polycistronic vector shown in panel A. The arrowhead indicates possible uncleaved product of H2B-iRFP-P2A-ERK-KTR-mKO. (D and E) Images before linear unmixing (D) and after linear unmixing (E) are represented in pseudo-color scale. HeLa cells transiently expressing each fluorescent protein (row) were imaged with each detection channel (column). Images placed top-left to bottom-right diagonally were taken with a suitable combination of fluorescent protein and filter set, and these average intensities are normalized to 1.0. The values shown in the images represent the fraction of fluorescence leakage compared with the image taken under a suitable filter condition. (F) Shown here are the representative unmixed images of Akt-FoxO3a-KTR-EGFP, ERK-KTR-mKO, mCherry-hGem, and H2B-iRFP obtained from HeLa cells stably expressing the four reporters by the polycistronic vector shown in panel B. Scale bar, 20 μ m.

FoxO3a to develop an Akt activity reporter, Akt-FoxO3a-KTR-EGFP. This biosensor exhibited clear change in the distribution from nucleus to cytoplasm under EGF administration, and it was completely suppressed by an Akt inhibitor, AZD5363 (Fig. 1D, right).

Interestingly, Akt-FoxO3a-KTR-EGFP accumulated in the nucleus upon Akt inhibitor treatment (Fig. 1D), suggesting that significant fraction of Akt-FoxO3a-KTR-EGFP was phosphorylated in the resting state. To examine the

phosphorylation site that contributes to the EGF-induced translocation and/or the cytoplasmic localization in the resting state, we generated two mutants of Akt-FoxO3a-KTR, Thr32Ala (T32A) and Ser315Ala (S315A) (Fig. 1E). The Akt-FoxO3a-KTR-T32A mutant localized at both cytosol and nucleus, as did Akt-FoxO3a-KTR WT. However, Akt-FoxO3a-KTR-T32A did not respond to EGF, indicating that Thr32 is the EGF-induced Akt phosphorylation site (Fig. 1E, left). Meanwhile, the Akt-FoxO3a-KTR-S315A

mutant localized predominantly in the nucleus, but still responded to EGF (Fig. 1E, right). Thus, substantial fraction of Ser315 is phosphorylated in an Akt-dependent manner to trap Akt-FoxO3a-KTR-EGFP in the cytoplasm.

Linear unmixing for multiplex imaging of ERK and Akt activities and cell cycle

We next developed a single-chain reporter for the nuclear localization, cell cycle, ERK activity, and Akt activity, which we named HGEA (Fig. 2A). This biosensor comprises the nuclear localization reporter Histone-H2B (H2B) fused with iRFP, the S/G₂/M cell-cycle reporter hGem (1/110) fused with mCherry (Sakaue-Sawano *et al.*, 2008b), ERK-KTR-mKO (Regot *et al.*, 2014), and Akt-FoxO3a-KTR-EGFP (Fig. 2B). The ERK-KTR consists of the KTR motif and the docking site for ERK, an LXL (DEJL) motif, which corresponds to the 312–356 a.a. region of Elk1. Each reporter is connected with a self-cleaving 2A peptide, P2A (Kim *et al.*, 2011) (Fig. 2B). HeLa cells stably expressing H2B-iRFP, mCherry-hGem, ERK-KTR-mKO, and Akt-FoxO3a-KTR-EGFP were established by cotransfection of pHGEA and the *piggyBac* transposon expression plasmid. Immunoblot analysis confirmed expression of each reporter that was cleaved out of the fusion protein (Fig. 2C). A faint 80 kDa protein was detected in the immunoblot with anti-mCherry antibody (Fig. 2C, left, arrow head). This 80 kDa protein was not detected by anti-KO antibody (Fig. 2C, center), suggesting that the P2A peptide between iRFP and mCherry may be partially resistant to cleavage. In conclusion, these data indicated reasonably high cleavage efficiency of P2A peptides (Fig. 2C).

For multi-color fluorescence imaging, we applied a linear unmixing approach to separate the spectral overlap of fluorescence signals among the four reporters (see Materials and Methods for details) (Hiraoka *et al.*, 2002; Niino *et al.*, 2009; Zimmermann *et al.*, 2003). The relative contribution of each fluorescent protein to each detection channel was determined by imaging HeLa cells transiently expressing individual fluorescent proteins with all filter sets (Fig. 2D). Before linear unmixing, a substantial amount of mKO fluorescence was detected with EGFP and mCherry channels (Fig. 2D), whereas the linear unmixing processing clearly discriminated the fluorescence leakage among fluorescent proteins (Fig. 2E). Further, H2B-iRFP, mCherry-hGem, ERK-KTR-mKO, and Akt-FoxO3a-KTR-EGFP demonstrated the expected subcellular localization after linear unmixing, ensuring the technical validity of the imaging procedure (Fig. 2F). As judged from the subcellular distribution of H2B-iRFP and mCherry-hGem, the uncleaved product, which was detected in the immunoblot analysis with anti-mCherry antibody, did not have little or no influence on both H2B-iRFP and mCherry-hGem signals. In the following section, all imaging data were processed by linear unmixing.

Specificity of ERK-KTR and Akt-FoxO3a-KTR

To confirm the specificity of ERK-KTR and Akt-FoxO3a-KTR, we applied a rapamycin-inducible dimerization system to ERK-KTR-mKO and Akt-FoxO3a-KTR-EGFP (Suh *et al.*, 2006). In this system, two fusion proteins, the rapamycin-binding domain of the FK506-binding protein (FKBP) fused to a specific signaling protein and the FK506-rapamycin-binding (FRB) domain of mTOR fused to the myristoylation signal of Lyn (Lyn11-FRB), are introduced into cells (Inoue *et al.*, 2005) (Fig. 3A and 3D). We used the full length CRaf protein and inter-*Src* homology 2 domain (iSH2) of the regulatory PI3K subunit p85, which are known to specifically activate the ERK and Akt pathways by their recruitment to the plasma membrane, respectively (Aoki *et al.*, 2011; Leever *et al.*, 1994; Miura *et al.*, 2014; Stokoe *et al.*, 1994; Suh *et al.*, 2006). Rapamycin treatment leads to rapid translocation of CRaf-FKBP and FKBP-iSH2 to the plasma membrane via heterodimerization of FKBP proteins and membrane-targeted Lyn11-FRB.

HeLa cells expressing the aforementioned four reporters and Lyn11-FRB and CRaf-FKBP demonstrated a rapid increase in the C/N ratios of ERK-KTR by rapamycin treatment, followed by a steep decrease through addition of the MEK inhibitor (Fig. 3B). The apparent on-rate and off-rate of ERK-KTR-mKO were 0.30 \pm 0.21 [1/min] and 0.13 \pm 0.13 [1/min], which were determined by fitting with a single exponential function, respectively. Akt-FoxO3a-KTR-EGFP exhibited a slight decrease in C/N ratios by ERK activation (Fig. 3C), suggesting negative feedback regulation of the Akt pathway by ERK. PI3K activation by rapamycin-induced membrane recruitment of FKBP-iSH2 caused transient increase in the C/N ratio of ERK-KTR, possibly via PI3K-Rac1-PAK-mediated ERK activation (Aksamitiene *et al.*, 2011; Fujita *et al.*, 2014) (Fig. 3E). The PI3K activation elevated the C/N ratios of Akt-FoxO3a-KTR, and this increase was suppressed by administrating AZD5363, an Akt inhibitor (Fig. 3F). In this experiment, the apparent on-rate and off-rate of Akt-FoxO3a-KTR-EGFP were 0.20 \pm 0.14 [1/min] and 0.062 \pm 0.049 [1/min], respectively.

p38 and JNK stress-activated protein kinase (SAPK) has been reported to contribute to redistribution of FoxO3a from the nucleus to cytoplasm (Clavel *et al.*, 2010). Therefore, we assessed the involvement of p38 and JNK in nucleocytoplasmic shuttling of ERK-KTR and Akt-FoxO3a-KTR. Anisomycin treatment, which induced p38 and JNK activation (Regot *et al.*, 2014), did not affect the C/N ratios of ERK-KTR-mKO and Akt-FoxO3a-KTR-EGFP (Fig. 3G and 3H). Neither the JNK inhibitor VIII nor SB203580 changed the C/N ratios of ERK-KTR-mKO (Fig. 3G) and Akt-FoxO3a-KTR-EGFP (Fig. 3H). From these data, we concluded that ERK-KTR and Akt-FoxO3a-KTR bear enough specificity to ERK and Akt activities, respectively.

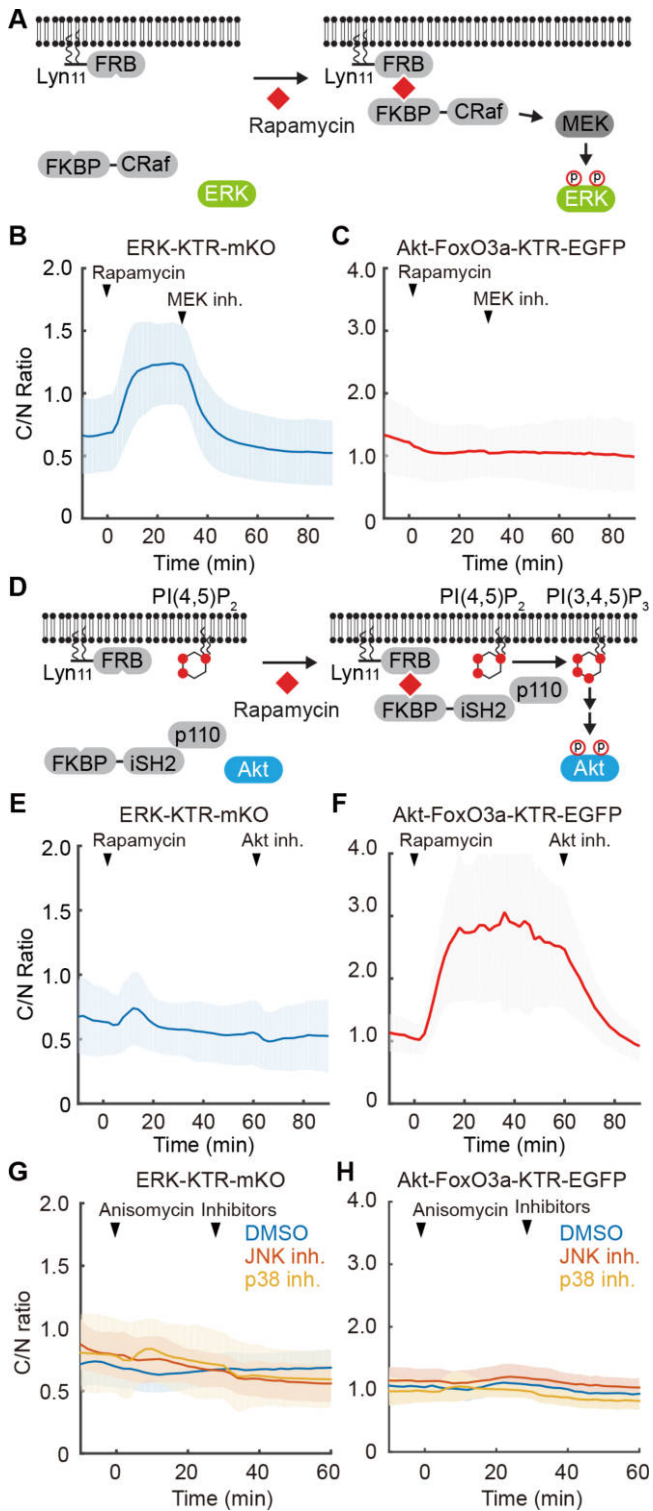


Fig. 3. Specificity of ERK-KTR and Akt-FoxO3a-KTR. (A) The schematic shows the rapamycin-induced ERK activation system by recruiting FKBP-CRaf to the plasma membrane through heterodimerization of Lyn11-FRB. (B and C) The rapamycin-induced ERK activation system was transiently introduced into HeLa cells stably expressing Akt-FoxO3a-KTR-EGFP, ERK-KTR-mKO, mCherry-hGem, and H2B-iRFP by the polycistronic vector. The cells were serum-starved for 3 hours. The cytoplasm-to-nuclear (C/N) ratios of ERK-KTR-mKO (B) and Akt-FoxO3a-KTR-EGFP (C) are plotted against time after 50 nM rapamycin treatment, followed by treatment with 10 μ M of an MEK inhibitor, PD184352. Data represent the mean \pm SD of more than 50 cells. (D) Schematic representation of the rapamycin-inducible PI3K activation system. (E and F) The rapamycin-induced Akt activation system was transiently introduced into HeLa cells as in panel D. The cells were serum-starved for 3 hours. The C/N ratios of ERK-KTR-mKO (E) and Akt-FoxO3a-KTR-EGFP (F) are plotted as a function of time after 50 nM rapamycin treatment, followed by treatment with 10 μ M of an Akt inhibitor, AZD5363. Data represent the mean \pm SD of more than 50 cells. (G and H) HeLa cells stably expressing Akt-FoxO3a-KTR-EGFP, ERK-KTR-mKO, mCherry-hGem, and H2B-iRFP were stimulated with 1.0 μ g/mL anisomycin with or without 10 μ M JNK inhibitor VIII or 10 μ M SB203580. The C/N ratios of ERK-KTR-mKO (G) and Akt-FoxO3a-KTR-EGFP (H) are plotted against time after anisomycin treatment. All data represent the mean \pm SD of more than 50 cells.

Sensitivity of ERK-KTR and Akt-FoxO3a-KTR

We next examined the sensitivity and dynamic range of ERK-KTR and Akt-FoxO3a-KTR. ERK-KTR-mKO dem-

onstrated nuclear exclusion in a manner dependent on EGF concentration (Fig. 4A). Under the same condition, endogenous ERK1/2 showed dual phosphorylation at threonine and tyrosine residues within the activation loop (Thr202

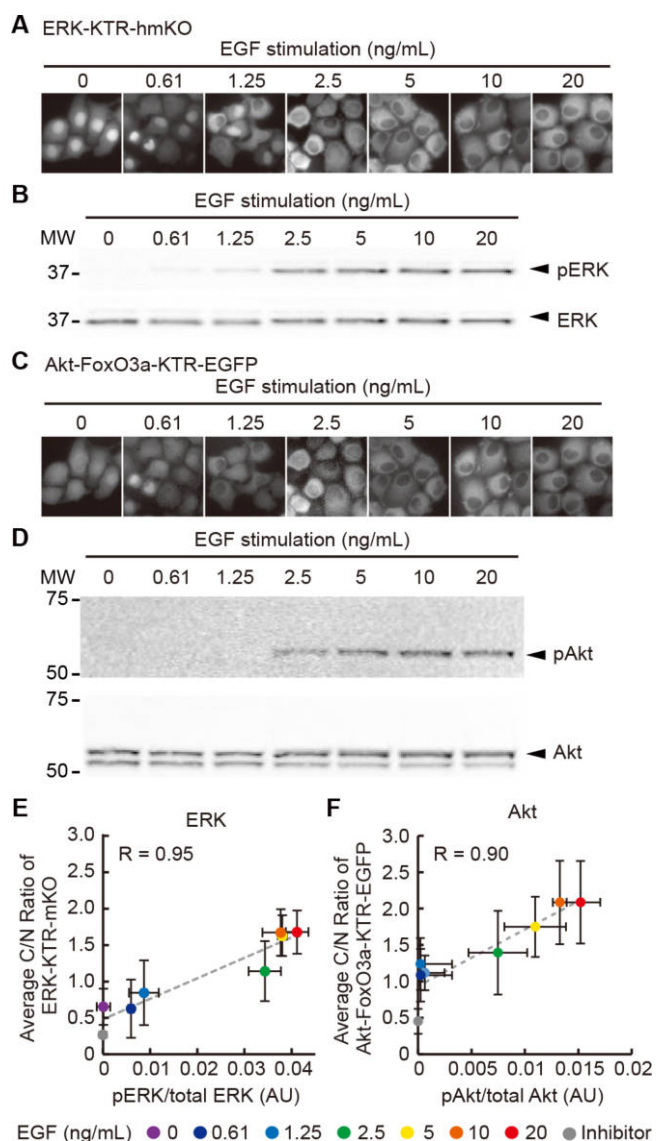


Fig. 4. Sensitivity of ERK-KTR and Akt-FoxO3a-KTR. (A–D) HeLa cells stably expressing Akt-FoxO3a-KTR-EGFP, ERK-KTR-mKO, mCherry-hGem, and H2B-iRFP were stimulated with the indicated concentration of EGF for 10 min, imaged for ERK-KTR-mKO (A) and Akt-FoxO3a-KTR-EGFP (C), or lysed in lysis buffer, followed by immunoblot analysis with pERK and ERK (B) or pAkt and Akt (D). Immunoblot images are representative of three independent experiments. (E and F) Average C/N ratios of ERK-KTR-mKO (E) and Akt-FoxO3a-KTR-EGFP (F) with the SD ($n > 10$ for all data point) are plotted as a function of the average pERK/ERK (E) and pAkt/Akt (F) values with the SD ($n = 3$), respectively. The dashed lines are the fitted lines, and R is the correlation coefficient.

and Tyr204/Thr185 and Tyr187), which are required for kinase activity of ERK (Chang and Karin, 2001; Qi and Elion, 2005), in a graded manner (Fig. 4B). EGF-induced nuclear exclusion of Akt-FoxO3a-KTR-EGFP was also analyzed in parallel with endogenous Akt phosphorylation (Ser473), which leads to full activation of Akt (Sarbasov *et al.*, 2005) (Fig. 4C and 4D). Based on these data, we directly compared the C/N ratios of individual KTRs with the phosphorylation levels of target kinases, and found that the C/N ratios of ERK-KTR-mKO and Akt-FoxO3a-KTR-EGFP were almost linearly correlated with the phosphorylation levels of ERK and Akt, respectively (Fig. 4E and 4F). Taken together with the data for specificity (Fig. 3), these results showed that ERK-KTR and Akt-FoxO3a-KTR demonstrated high specificity and sensitivity to ERK and Akt activities, respectively.

Cell-cycle-dependent dynamic regulation of ERK and Akt upon EGF stimulation

Finally, we investigated how ERK and Akt are cooperatively regulated upon EGF stimulation in living cells. EGF stimulation resulted in the translocation of ERK-KTR-mKO and Akt-FoxO3a-KTR-EGFP from nucleus to cytoplasm, and thereafter, PD184352 and AZD5363 treatment abolished their cytoplasmic translocation, respectively (Fig. 5A and 5B). Cell-to-cell heterogeneity of ERK activity, Akt activity and cell-cycle status are shown in heatmaps under the three conditions; EGF→DMSO treatment, EGF→Akt-inhibitor treatment, and EGF→MEK inhibitor treatment (Fig. 5C–5E). The data of each cell are aligned vertically in accordance with the cell-cycle status from early G_1 to S/ G_2 /M (from top to bottom) (Fig. 5C–5E, right). Although

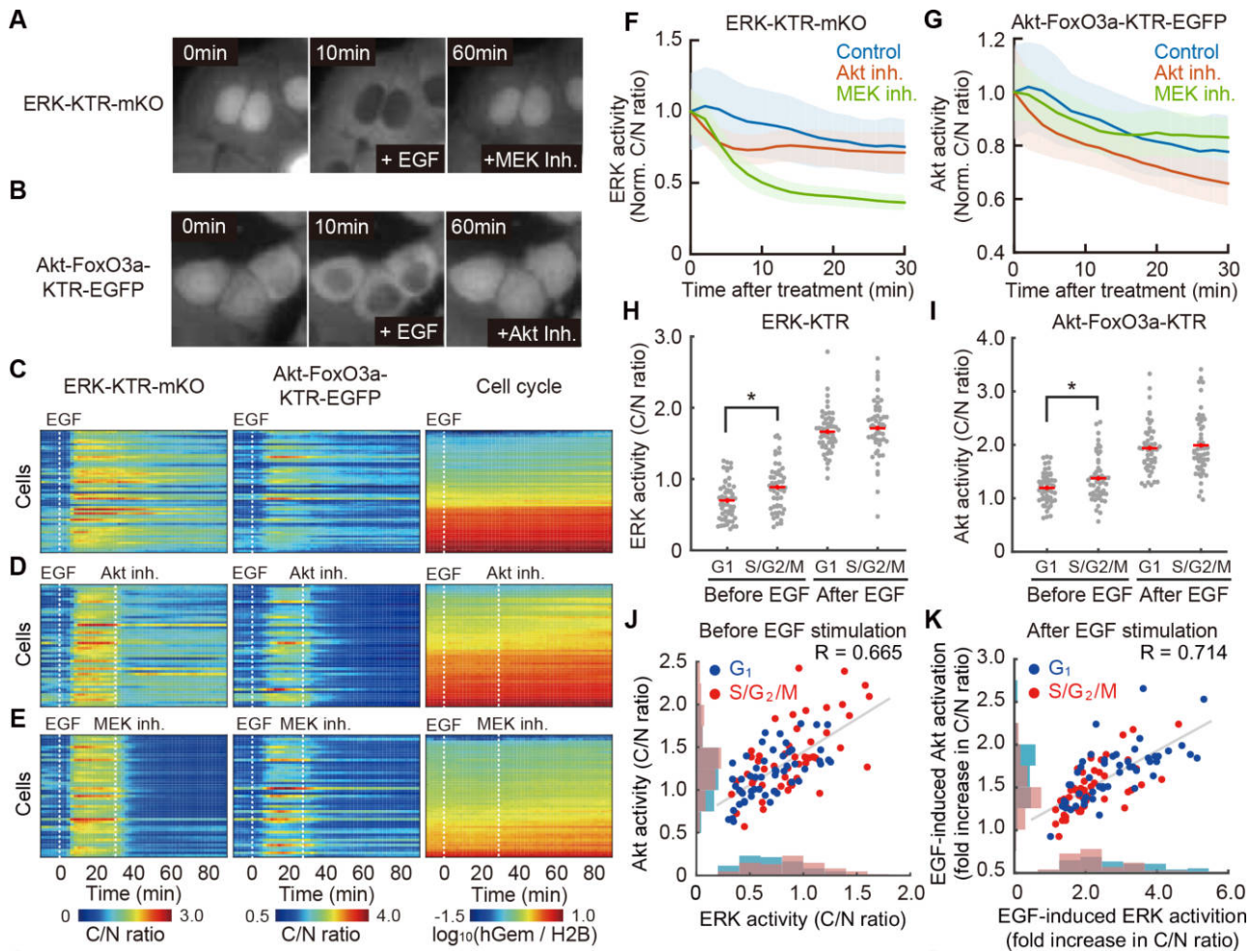


Fig. 5. Cell-cycle-dependence of the EGF-induced activation of ERK and Akt. (A and B) HeLa cells stably expressing Akt-FoxO3a-KTR-EGFP, ERK-KTR-mKO, mCherry-hGem, and H2B-iRFP were stimulated with the indicated concentration of 10 ng/mL EGF for 10 min, followed by the addition of an MEK inhibitor (10 μ M PD184352) (A) or Akt inhibitor (20 μ M AZD5363). Representative images of ERK-KTR-mKO (A) and Akt-FoxO3a-KTR-EGFP (B) are shown. (C–D) HeLa cells were serum-starved for 3 hours, and stimulated with EGF alone (C), EGF and Akt inhibitor (D), or EGF and MEK inhibitor (E), and imaged as in panels A and B. The ERK activity (C/N ratios of ERK-KTR-mKO, left), Akt activity (C/N ratios of Akt-FoxO3a-KTR-EGFP, middle), and cell-cycle status (\log_{10} (hGem-mCherry/H2B-iRFP)) are represented as heatmaps. Each row of the heatmaps corresponds to an individual cell, which are sorted by cell-cycle status from G₁ to S/G₂/M cells (from top to bottom) ($n > 50$). (F and G) The C/N ratios of ERK-KTR (F) and Akt-FoxO3a-KTR (G) are normalized to the average C/N ratio values at the time of inhibitor treatment, and plotted as a function of time after inhibitor treatment with SD. (H and I) The C/N ratios of ERK-KTR (H) and Akt-FoxO3a-KTR (I) are plotted before (0 min) and after EGF addition (10 min). G₁ cells and S/G₂/M are defined as the lower 33% and higher 33% of hGem-mCherry/H2B-iRFP values, respectively. The red line indicates the mean value. The symbols indicate the results of Welch's *t* test analysis; * $p < 0.05$. (J) The C/N ratios of Akt-FoxO3a-KTR in G₁ cells (blue dot) and S/G₂/M cells (orange dot) are plotted against the C/N ratios of ERK-KTR before EGF stimulation with a fitted line (gray line) and correlation coefficient, R. Histograms of fold-increase in ERK activity (horizontal axis) and Akt activity (vertical axis) of G₁ cells (blue) and S/G₂/M cells (red) are included in the scatter plot. (K) Fold-increase values of the C/N ratios of Akt-FoxO3a-KTR by EGF stimulation are plotted as a function of fold-increase values of the C/N ratios of ERK-KTR with a fitted line (gray line) and correlation coefficient, R. Histograms of fold-increase in ERK activity (horizontal axis) and Akt activity (vertical axis) of G₁ cells (blue) and S/G₂/M cells (red) are included in the scatter plot.

significant variance was observed among cells, ERK-KTR and Akt-FoxO3a-KTR generally exhibited a quick increase in their C/N ratios after EGF stimulation, followed by a gradual decrease (Fig. 5C).

We focused on the response of ERK-KTR and Akt-FoxO3a-KTR to each inhibitor to clarify the cross-talk regulations between ERK and Akt signaling. As expected,

ERK was rapidly and continually suppressed by the MEK inhibitor (Fig. 5F, green line). Treatment with the Akt inhibitor transiently suppressed ERK activity in the early phase (<10 min after addition of inhibitor), while ERK activity remained at sustained levels or was even partially recovered in the late phase of Akt inhibitor treatment (>10 min) (Fig. 5F, red line). In agreement with this finding, a

transient reduction of ERK activity by PI3K inhibitor treatment has also been observed by FRET imaging (Fujita *et al.*, 2014). This result could be due to the combination of cross-talk activation of ERK mediated by the PI3K-Akt-PAK-Raf pathway in the early phase (Aksamitiene *et al.*, 2011), followed by the feedback inhibition of EGFR by ERK in the late phase (Sato *et al.*, 2013). Akt activity was suppressed by the treatment with the Akt inhibitor (Fig. 5G, red line). We observed slight but reproducible up-regulation of Akt activity following treatment with the MEK inhibitor in the late phase (>20 min) (Fig. 5G, green line), suggesting the cross-talk inhibition of Akt by ERK signaling through EGFR (Sato *et al.*, 2013) and/or Sos1 (Kamioka *et al.*, 2010). Intriguingly, we found some evidences that ERK and Akt are coordinately regulated in a cell-cycle-dependent manner. First, we defined cells showing in the lower 33% and higher 33% of hGem-mCherry/H2B-iRFP values as G₁ cells and S/G₂/M cells, respectively. Basal ERK and Akt activities in the absence of EGF in S/G₂/M cells were significantly higher than those in G₁ cells (Fig. 5H and 5I). The peak values of the C/N ratios of ERK-KTR and Akt-FoxO3a-KTR did not show any statistically significant difference between G₁ cells and S/G₂/M cells (Fig. 5H and 5I). Next, we plotted the C/N ratios of Akt-FoxO3a-KTR against the C/N ratios of ERK-KTR in individual cells under the basal condition, and observed a clear correlation between ERK activity and Akt activity (Fig. 5J). The difference of ERK activity and Akt activity between G₁ cells and S/G₂/M cells was also manifested in this graph. Further, EGF-induced ERK activation was also correlated with EGF-induced Akt activation (Fig. 5K). The S/G₂/M cells demonstrated a lower activation level of ERK and Akt upon EGF stimulation than those in G₁ cells. This could have been due to the higher basal level of ERK and Akt activities in S/G₂/M cells. This data appeared to be consistent with the previous observation that Ras was not activated in S/G₂/M cells upon EGF stimulation (Sakaue-Sawano *et al.*, 2008a). Taken together, these data indicated that ERK and Akt are co-regulated in each cell, and this coordinated regulation of ERK and Akt is modulated in cell-cycle progression.

Discussion

In this study, we established a multiplexed imaging system for monitoring ERK and Akt activities. Our system enabled us to visualize ERK and Akt activities and the cell-cycle progression quantitatively and simultaneously in a live cell, and provided insight into the cellular heterogeneity and cross-talk regulation between the Ras-ERK and PI3K-Akt pathways, which has not been readily assessed by conventional biochemical methods.

In a comparison with previously developed Akt biosensors, Akt-FoxO3a-KTR had characteristic advantages, *e.g.*,

it is fused with a single fluorescent protein and easily quantified. The most notable advantage, however, is its sensitivity; there was an approximately 1.5–2.0 fold increase in the C/N ratios of Akt-FoxO3a-KTR-EGFP upon EGF stimulation (Fig. 5K). Under the same condition, the FRET biosensors for Akt activity, Eevee-iAkt, Eevee-Akt-cyt, Aktus, BKAR, and Akind, exhibited only a 1.03–1.1 fold increase in FRET/CFP ratios (Komatsu *et al.*, 2011; Kunkel *et al.*, 2005; Miura *et al.*, 2014; Sasaki *et al.*, 2003; Yoshizaki *et al.*, 2007). This higher sensitivity could be attributed to the structure of Akt-FoxO3a-KTR, which includes almost half of FoxO3a from the N-terminus (1–402 a.a.). We assume that there exists an Akt docking domain in this region, and thereby, Akt-FoxO3a-KTR is more efficiently phosphorylated by Akt than other FRET biosensors, most of which contain only a few amino acids in an Akt phosphorylation site (Komatsu *et al.*, 2011; Kunkel *et al.*, 2005; Miura *et al.*, 2014; Sasaki *et al.*, 2003). Indeed, we found the two phosphorylation sites of Akt-FoxO3a-KTR, Thr32 and Ser315, which accounted for changes in subcellular distribution of Akt-FoxO3a-KTR in a manner dependent on stimulation-induced and basal PI3K/Akt signals, respectively (Fig. 1C–E). The molecular mechanisms underlying two modes of Akt-FoxO3a-KTR regulated by different phosphorylation sites remain unclear. There are also some disadvantages to be considered when attempting to use Akt-FoxO3a-KTR to measure Akt activity. First, the critical drawback of Akt-FoxO3a-KTR compared to other FRET-based biosensors is that Akt-FoxO3a-KTR cannot visualize subcellular Akt activity, because the KTR system is completely reliant on the nuclear import and export of the reporters (Regot *et al.*, 2014). Second, the apparent time constants of the on-rate and off-rate of Akt-FoxO3a-KTR-EGFP (3 min and 16 min, respectively) are slower than those of Eevee-iAkt (both ca. 2 min) (Miura *et al.*, 2014). On the other hand, ERK-KTR and JNK-KTR showed relatively rapid responses to their stimuli (Regot *et al.*, 2014) (Fig. 3). This discrepancy was attributed to the difference of nuclear translocation of kinases; we could not observe EGF-induced Akt activation at the nucleus (Miura *et al.*, 2014), while activated ERK and JNK are well known to translocate to the nucleus, so that ERK-KTR and JNK-KTR at the nucleus are phosphorylated and exported quickly.

Our data demonstrated that ERK-KTR and Akt-FoxO3a-KTR monitor ERK and Akt activities with high specificity, respectively. ERK-KTR contains an LXL (DEJL) motif of Elk1, which is bound to ERK and JNK, and phosphorylated by ERK, p38 and JNK (Marais *et al.*, 1993). Nonetheless, anisomycin did not change the C/N ratios of ERK-KTR (Fig. 3G). On the other hand, rapamycin-induced ERK activation slightly decreased the C/N ratios of Akt-FoxO3a-KTR, followed by an increase in the C/N ratios of Akt-FoxO3a-KTR upon MEK inhibitor treatment (Fig. 3C). This may have been due to the negative feedback from ERK to Akt through EGFR (Fujita *et al.*, 2014; Kamioka *et*

al., 2010; Sato *et al.*, 2013). It has been reported that ERK phosphorylates FoxO3a at Ser294, Ser344 and Ser425, and induces nuclear export and ubiquitination of FoxO3a (Yang *et al.*, 2008). However, we could not find any observations supporting ERK-mediated nucleocytoplasmic shuttling of Akt-FoxO3a -KTR. Further improvements and characterizations, e.g., deletion of ERK phosphorylation sites, will be necessary to accurately visualize Akt activity with Akt-FoxO3a-KTR in a future study.

This study provides insights into the cellular heterogeneity of ERK and Akt activities. Our data demonstrated the strong positive correlations between ERK activity and Akt activity in the basal state and responsiveness to EGF stimulation at the single cell level (Fig. 5J and 5K). Many receptor tyrosine kinases such as EGFR and PDGFR are known to concomitantly activate both the Ras-ERK pathway and PI3K-Akt pathway (Yarden and Sliwkowski, 2001). It is possible that the expression level and/or degradation rate of RTKs that activate both ERK and Akt are regulated in individual cells, leading to the emergence of cellular heterogeneity for ERK and Akt activities.

That the ERK and Akt activities of cells in the S/G₂/M phase are higher than those in the G₁ phase implies that these activities play synergistic roles in S/G₂/M progression. ERK and Akt are classically considered to play a role in G₁/S progression through mechanisms such as an increase in cyclin D1 expression (Sears and Nevins, 2002; Torii *et al.*, 2006). However, a role of ERK and Akt in G₂/M progression has also been reported in cultured cells (Liang and Slingerland, 2003; Tamemoto *et al.*, 1992; Wang *et al.*, 2007; Wright *et al.*, 1999). More recently, we revealed the intercellular propagation of ERK and its role in S/G₂/M transition (Hiratsuka *et al.*, 2015) with *in vivo* imaging of ERK activity in transgenic mice expressing an ERK FRET biosensor (Kamioka *et al.*, 2012). It is still unclear which signaling molecules maintained the higher ERK and Akt activities in the S/G₂/M phase, and how ERK and Akt cooperatively regulated G₂/M progression.

In summary, we developed and characterized a multiplexed system for imaging ERK and Akt activities and the cell-cycle progression, and demonstrated cell-cycle-dependent heterogeneity of ERK and Akt activities at the single cell level. ERK-dependent upregulation of mTORC1, which is a downstream molecule of Akt, is closely associated with intrinsic resistance to MEK inhibitors in KRas- or BRaf-mutant cancer cells (Komatsu *et al.*, 2015). Thus, our system will provide a useful tool to quantitatively evaluate the relationship between ERK and Akt activities and intrinsic resistance to molecularly targeted drugs for Ras-ERK and/or PI3K-Akt pathways in cancer cells.

Acknowledgments. We thank Dr. Miyawaki (Fucci), Dr. Miyoshi (pCSII), and Dr. Miyanari (H2B-iRFP) for providing the plasmids. We are grateful to the members of the Matsuda Laboratory for their helpful input. Y Inaoka, K Hirano, N Nishimoto, and A Kawagishi are to be thanked for their technical assistance. KA and MM were supported by the Platform for

Dynamic Approaches to Living System from the Ministry of Education, Culture, Sports, Science and Technology, Japan. KA was supported by a Grant-in-Aid for Scientific Research (B) (80511427). MM was supported by Grants-in-Aid for Scientific Research (15H02397 and 15H0594). GM was supported by the Mitsubishi UFJ Trust Scholarship Foundation.

Conflict of interest

The authors declare that there is no conflict of interest.

References

- Ai, H., Hazelwood, K.L., Davidson, M.W., and Campbell, R.E. 2008. Fluorescent protein FRET pairs for ratiometric imaging of dual biosensors. *Nat. Methods*, **5**: 401–403.
- Aksamitiene, E., Achanta, S., Kolch, W., Kholodenko, B.N., Hoek, J.B., and Kiyatkin, A. 2011. Prolactin-stimulated activation of ERK1/2 mitogen-activated protein kinases is controlled by PI3-kinase/Rac/PAK signaling pathway in breast cancer cells. *Cell. Signal.*, **23**: 1794–1805.
- Aoki, K., Yamada, M., Kunida, K., Yasuda, S., and Matsuda, M. 2011. Processive phosphorylation of ERK MAP kinase in mammalian cells. *Proc. Natl. Acad. Sci. USA*, **108**: 12675–12680.
- Brunet, A., Bonni, A., Zigmond, M.J., Lin, M.Z., Juo, P., Hu, L.S., Anderson, M.J., Arden, K.C., Blenis, J., and Greenberg, M.E. 1999. Akt promotes cell survival by phosphorylating and inhibiting a Forkhead transcription factor. *Cell*, **96**: 857–868.
- Chang, L. and Karin, M. 2001. Mammalian MAP kinase signalling cascades. *Nature*, **410**: 37–40.
- Clavel, S., Siffroi-Fernandez, S., Coldefy, A.S., Boulukos, K., Pisani, D.F., and Dérijard, B. 2010. Regulation of the intracellular localization of Foxo3a by stress-activated protein kinase signaling pathways in skeletal muscle cells. *Mol. Cell. Biol.*, **30**: 470–480.
- Friday, B.B., Yu, C., Dy, G.K., Smith, P.D., Wang, L., Thibodeau, S.N., and Adjei, A.A. 2008. BRAF V600E disrupts AZD6244-induced abrogation of negative feedback pathways between extracellular signal-regulated kinase and Raf proteins. *Cancer Res.*, **68**: 6145–6153.
- Fujita, Y., Komatsu, N., Matsuda, M., and Aoki, K. 2014. Fluorescence resonance energy transfer based quantitative analysis of feedforward and feedback loops in epidermal growth factor receptor signaling and the sensitivity to molecular targeting drugs. *FEBS J.*, **281**: 3177–3192.
- Hiraoka, Y., Shimi, T., and Haraguchi, T. 2002. Multispectral imaging fluorescence microscopy for living cells. *Cell Struct. Funct.*, **27**: 367–374.
- Hiratsuka, T., Fujita, Y., Naoki, H., Aoki, K., Kamioka, Y., and Matsuda, M. 2015. Intercellular propagation of extracellular signal-regulated kinase activation revealed by *in vivo* imaging of mouse skin. *Elife*, **2015**: 1–18.
- Hu, M.C.T., Lee, D.F., Xia, W., Golfman, L.S., Ou-Yang, F., Yang, J.Y., Zou, Y., Bao, S., Hanada, N., Saso, H., *et al.* 2004. IκB kinase promotes tumorigenesis through inhibition of forkhead FOXO3a. *Cell*, **117**: 225–237.
- Inoue, T., Heo, W. Do, Grimley, J.S., Wandless, T.J., and Meyer, T. 2005. An inducible translocation strategy to rapidly activate and inhibit small GTPase signaling pathways. *Nat. Methods*, **2**: 415–418.
- Inoue, T. and Meyer, T. 2008. Synthetic activation of endogenous PI3K and Rac identifies an AND-gate switch for cell polarization and migration. *PLoS One*, **3**: e3068.
- Kamioka, Y., Yasuda, S., Fujita, Y., Aoki, K., and Matsuda, M. 2010. Multiple decisive phosphorylation sites for the negative feedback regulation of SOS1 via ERK. *J. Biol. Chem.*, **285**: 33540–33548.
- Kamioka, Y., Sumiyama, K., Mizuno, R., Sakai, Y., Hirata, E., Kiyokawa, E., and Matsuda, M. 2012. Live Imaging of Protein Kinase Activities in Transgenic Mice Expressing FRET Biosensors. *Cell Struct. Funct.*, **37**:

- 65–73.
- Kim, J.H., Lee, S.R., Li, L.H., Park, H.J., Park, J.H., Lee, K.Y., Kim, M.K., Shin, B.A., and Choi, S.Y. 2011. High cleavage efficiency of a 2A peptide derived from porcine teschovirus-1 in human cell lines, zebrafish and mice. *PLoS One*, **6**: e18556.
- Komatsu, N., Aoki, K., Yamada, M., Yukinaga, H., Fujita, Y., Kamioka, Y., and Matsuda, M. 2011. Development of an optimized backbone of FRET biosensors for kinases and GTPases. *Mol. Biol. Cell*, **22**: 4647–4656.
- Komatsu, N., Fujita, Y., Matsuda, M., and Aoki, K. 2015. mTORC1 upregulation via ERK-dependent gene expression change confers intrinsic resistance to MEK inhibitors in oncogenic KRas-mutant cancer cells. *Oncogene*, **34**: 3985–3993.
- Kunkel, M.T., Ni, Q., Tsien, R.Y., Zhang, J., and Newton, A.C. 2005. Spatio-temporal dynamics of protein kinase B/Akt signaling revealed by a genetically encoded fluorescent reporter. *J. Biol. Chem.*, **280**: 5581–5587.
- Leever, S.J., Paterson, H.F., and Marshall, C.J. 1994. Requirement for Ras in Raf activation is overcome by targeting Raf to the plasma membrane. *Nature*, **369**: 411–414.
- Lehr, S., Kotzka, J., Avci, H., Sickmann, A., Meyer, H.E., Herkner, A., and Muller-Wieland, D. 2004. Identification of major ERK-related phosphorylation sites in Gab1. *Biochemistry*, **43**: 12133–12140.
- Liang, J. and Slingerland, J.M. 2003. Multiple Roles of the PI3K/PKB (Akt) Pathway in Cell Cycle Progression. *Cell Cycle*, **2**: 336–342.
- Marais, R., Wynne, J., and Treisman, R. 1993. The SRF accessory protein Elk-1 contains a growth factor-regulated transcriptional activation domain. *Cell*, **73**: 381–393.
- Mendoza, M.C., Er, E.E., and Blenis, J. 2011. The Ras-ERK and PI3K-mTOR pathways: cross-talk and compensation. *Trends Biochem. Sci.*, **36**: 320–328.
- Miura, H., Matsuda, M., and Aoki, K. 2014. Development of a FRET biosensor with high specificity for Akt. *Cell Struct. Funct.*, **39**: 9–20.
- Niino, Y., Hotta, K., and Oka, K. 2009. Simultaneous live cell imaging using dual FRET sensors with a single excitation light. *PLoS One*, **4**: e6036.
- Obsil, T. and Obsilova, V. 2008. Structure/function relationships underlying regulation of FOXO transcription factors. *Oncogene*, **27**: 2263–2275.
- Polivka Jr., J. and Janku, F. 2014. Molecular targets for cancer therapy in the PI3K/AKT/mTOR pathway. *Pharmacol. Ther.*, **142**: 164–175.
- Prahallad, A., Sun, C., Huang, S., Di Nicolantonio, F., Salazar, R., Zecchin, D., Beijersbergen, R.L., Bardelli, A., and Bernards, R. 2012. Unresponsiveness of colon cancer to BRAF(V600E) inhibition through feedback activation of EGFR. *Nature*, **483**: 100–103.
- Pylayeva-Gupta, Y., Grabocka, E., and Bar-Sagi, D. 2011. RAS oncogenes: weaving a tumorigenic web. *Nat. Rev. Cancer*, **11**: 761–774.
- Qi, M. and Elion, E.A. 2005. MAP kinase pathways. *J. Cell Sci.*, **118**: 3569–3572.
- Regot, S., Hughey, J.J., Bajar, B.T., Carrasco, S., and Covert, M.W. 2014. High-sensitivity measurements of multiple kinase activities in live single cells. *Cell*, **157**: 1724–1734.
- Roberts, P. and Der, C. 2007. Targeting the Raf-MEK-ERK mitogen-activated protein kinase cascade for the treatment of cancer. *Oncogene*, **26**: 3291–3310.
- Sakaue-Sawano, A., Kurokawa, H., Morimura, T., Hanyu, A., Hama, H., Osawa, H., Kashiwagi, S., Fukami, K., Miyata, T., Miyoshi, H., *et al.* 2008a. Visualizing Spatiotemporal Dynamics of Multicellular Cell-Cycle Progression. *Cell*, **132**: 487–498.
- Sakaue-Sawano, A., Ohtawa, K., Hama, H., Kawano, M., Ogawa, M., and Miyawaki, A. 2008b. Tracing the Silhouette of Individual Cells in S/G2/M Phases with Fluorescence. *Chem. Biol.*, **15**: 1243–1248.
- Sarbassov, D.D., Guertin, D.A., Ali, S.M., and Sabatini, D.M. 2005. Phosphorylation and regulation of Akt/PKB by the rictor-mTOR complex. *Science*, **307**: 1098–1101.
- Sasaki, K., Sato, M., and Umezawa, Y. 2003. Fluorescent indicators for Akt/protein kinase B and dynamics of Akt activity visualized in living cells. *J. Biol. Chem.*, **278**: 30945–30951.
- Sato, K., Shin, M.S., Sakimura, A., Zhou, Y., Tanaka, T., Kawanishi, M., Kawasaki, Y., Yokoyama, S., Koizumi, K., Saiki, I., *et al.* 2013. Inverse correlation between Thr-669 and constitutive tyrosine phosphorylation in the asymmetric epidermal growth factor receptor dimer conformation. *Cancer Sci.*, **104**: 1315–1322.
- Sears, R.C. and Nevins, J.R. 2002. Signaling networks that link cell proliferation and cell fate. *J. Biol. Chem.*, **277**: 11617–11620.
- She, Q.B., Chandarlapaty, S., Ye, Q., Lobo, J., Haskell, K.M., Leander, K.R., DeFeo-Jones, D., Huber, H.E., and Rosen, N. 2008. Breast tumor cells with PI3K mutation or HER2 amplification are selectively addicted to Akt signaling. *PLoS One*, **3**: e3065.
- Stokoe, D., Macdonald, S.G., Cadwallader, K., Symons, M., and Hancock, J.F. 1994. Activation of Raf as a result of recruitment to the plasma membrane. *Science*, **264**: 1463–1477.
- Suh, B.-C., Inoue, T., Meyer, T., and Hille, B. 2006. Rapid chemically induced changes of PtdIns(4,5)P2 gate KCNQ ion channels. *Science*, **314**: 1454–1457.
- Tamemoto, H., Kadowaki, T., Tobe, K., Ueki, K., Izumi, T., Chatani, Y., Kohno, M., Kasuga, M., Yazaki, Y., and Akanuma, Y. 1992. Biphasic activation of two mitogen-activated protein kinases during the cell cycle in mammalian cells. *J. Biol. Chem.*, **267**: 20293–20297.
- Torii, S., Yamamoto, T., Tsuchiya, Y., and Nishida, E. 2006. ERK MAP kinase in G cell cycle progression and cancer. *Cancer Sci.*, **97**: 697–702.
- Tran, H., Brunet, A., Grenier, J.M., Datta, S.R., Fornace, A.J., DiStefano, P.S., Chiang, L.W., and Greenberg, M.E. 2002. DNA repair pathway stimulated by the forkhead transcription factor FOXO3a through the Gadd45 protein. *Science*, **296**: 530–534.
- Wang, R., He, G., Nelman-Gonzalez, M., Ashorn, C.L., Gallick, G.E., Stukenberg, P.T., Kirschner, M.W., and Kuang, J. 2007. Regulation of Cdc25C by ERK-MAP Kinases during the G2/M Transition. *Cell*, **128**: 1119–1132.
- Won, J.K., Yang, H.W., Shin, S.Y., Lee, J.H., Heo, W. Do, and Cho, K.H. 2012. The crossregulation between ERK and PI3K signaling pathways determines the tumoricidal efficacy of MEK inhibitor. *J. Mol. Cell Biol.*, **4**: 153–163.
- Wright, J.H., Munar, E., Jameson, D.R., Andreassen, P.R., Margolis, R.L., Seger, R., and Krebs, E.G. 1999. Mitogen-activated protein kinase activity is required for the G(2)/M transition of the cell cycle in mammalian fibroblasts. *Proc. Natl. Acad. Sci. USA*, **96**: 11335–11340.
- Yang, J.-Y., Zong, C.S., Xia, W., Yamaguchi, H., Ding, Q., Xie, X., Lang, J.-Y., Lai, C.-C., Chang, C.-J., Huang, W.-C., *et al.* 2008. ERK promotes tumorigenesis by inhibiting FOXO3a via MDM2-mediated degradation. *Nat. Cell Biol.*, **10**: 138–148.
- Yarden, Y. and Sliwkowski, M.X. 2001. Untangling the ErbB signalling network. *Nat. Rev. Mol. Cell Biol.*, **2**: 127–137.
- Yoshizaki, H., Mochizuki, N., Gotoh, Y., and Matsuda, M. 2007. Akt-PDK1 Complex Mediates EGF-induced Membrane Protrusion through Ral Activation. *Mol. Biol. Cell*, **18**: 119–128.
- Yusa, K., Rad, R., Takeda, J., and Bradley, A. 2009. Generation of transgene-free induced pluripotent mouse stem cells by the piggyBac transposon. *Nat. Methods*, **6**: 363–369.
- Zimmermann, S. and Moelling, K. 1999. Phosphorylation and regulation of Raf by Akt (protein kinase B). *Science*, **286**: 1741–1744.
- Zimmermann, T., Rietdorf, J., and Pepperkok, R. 2003. Spectral imaging and its applications in live cell microscopy. *FEBS Lett.*, **546**: 87–92.

(Received for publication, April 20, 2016, accepted, May 20, 2016
and published online, May 28, 2016)